Available online at www.sciencedirect.com
ScienceDirect
Journal of Sound and Vibration 321 (2009) 955–975
JOURNAL OF SOUND AND VIBRATION
www.elsevier.com/locate/jsvi

Nonlinear oscillations of automotive turbocharger turbines

Bernhard Schweizer[a,*], Mario Sievert[b]

[a]Department of Mechanical Engineering, Multibody Systems, University of Kassel, Mönchebergstr. 7, 34109 Kassel, Germany
[b]Voith Turbo Aufladungssysteme GmbH & Co. KG, Berliner Heerstraße 1c, 38104 Braunschweig, Germany

Received 12 February 2008; received in revised form 29 August 2008; accepted 8 October 2008
Handling Editor: C.L. Morfey
Available online 14 January 2009

Abstract

Turbines, especially turbines supported in hydrodynamic bearings, often exhibit interesting oscillation effects, which result from the bearing nonlinearities. In the present work, an automotive turbocharger rotor is investigated. The rotor of the turbocharger examined here is supported in full-floating ring bearings, which give rise to complex system vibrations. Frequency spectra of run-up measurements, carried out on a hot-gas turbocharger test rig, are presented. The occurring nonlinear effects—self-excited vibrations, *oil whirl/whip* phenomena, subharmonics, superharmonics, combination frequencies and jump phenomena—are explained in detail with the help of a gyroscopic eigenvalue analysis and by run-up simulations with a multibody model of the rotor/bearing system. The influence of different operating conditions—oil supply pressure, oil supply temperature and rotor imbalance—on the rotor oscillations and the system bifurcations is studied.

1. Introduction

Nonlinear vibrations play an important role in many technical applications. Sometimes, the system nonlinearities are weak so that the system still behaves mainly linear. In many applications, however, the system is dominated by nonlinear effects. In this case, it is not useful to linearize the system in order to examine the system dynamics.

The mechanical system studied in this work, namely a turbocharger rotor supported in two full-floating ring bearings, exhibit a highly nonlinear behavior. Often in rotor dynamics, the system can be linearized in order to calculate the vibrations of the rotor as well as to analyze the stability of the rotor/bearing system [1–3]. For the turbocharger investigated here, this is not suitable. As known from literature, high-speed turbines in full-floating ring bearings perform—over a wide part of the rotor speed range—different types of limit cycles oscillations, which are caused by *oil whirl* and *oil whip* instabilities generated by the inner and outer oil films of the floating ring bearings [4–11].

Oil whirl and *oil whip* instabilities, inducing self-excited limit cycle oscillations in rotor systems, have been thoroughly examined in literature. Analytical, numerical and experimental investigations on this subject can

*Corresponding author. Tel.: +49 561 804 3259; fax: +49 561 804 2847.
E-mail address: schweizer@mks.uni-kassel.de (B. Schweizer).

0022-460X/$ - see front matter © 2008 Elsevier Ltd. All rights reserved.
doi:10.1016/j.jsv.2008.10.013

be found in Refs. [12–18]. An overview on nonlinear vibration effects, occurring in dynamical systems, is given in Refs. [19–21].

In the current paper, run-up measurements of a turbocharger rotor supported in full-floating ring bearings are presented. Crucial operating and system parameters are systematically varied in order to detect their influence on the dynamics and especially on the bifurcation behavior of the system. The presented frequency spectra and their explanation/interpretation may be valuable and helpful for both, interested readers in nonlinear rotor dynamics and readers involved with bifurcation and stability theory. The measurements show interesting vibration effects and phenomena, not reported in earlier publications on rotor systems with floating ring bearings: In Measurement 3 and particularly in Measurement 6, for instance, we observed the astonishing phenomenon of a limit cycle oscillation locking at a subsynchronous frequency. In Measurement 2, the state of both rings (at rest or rotating) can be detected indirectly, since the frequency spectrum shows two different limit cycle frequencies, resulting from the inner *oil whirl* of the compressor-sided and turbine-sided ring. A main intention of the paper is to mechanically interpret the occurring nonlinear dynamical effects in order to get a closer insight into the complex nonlinear oscillation behavior of such systems. The examined turbocharger exhibits different bifurcations, self-excited vibrations, jump phenomena and locking effects. These effects are mechanically investigated and explained in detail by means of a gyroscopic eigenfrequency analysis of the turbocharger rotor and by run-up simulations with a multibody model of the rotor/bearing system.

In Section 2 of the paper, the investigated turbocharger rotor is described and a gyroscopic eigenvalue analysis is carried out for the rotor/bearing system, too. Test rig measurements are presented in Section 3. The work is summarized in Section 4. A short recapitulation of the *oil whirl* and *oil whip* phenomena is given in Appendix A for both, a Jeffcott rotor in plain hydrodynamic bearings and a Jeffcott rotor in full-floating ring bearings. In addition, results of a turbocharger run-up simulation are shown and briefly discussed.

2. System description

Turbochargers are essential components in combustion engines. They are used in connection with diesel and gasoline engines. The operating principle is quite easy (Fig. 1). The thermal energy of the exhaust gas causes the turbine wheel to rotate. At the same time, the compressor wheel compresses ambient air for the intake of the engine. The more air is compressed, the higher the amount of fuel/air mixture entering the cylinder of the combustion engine is. In this work, a turbocharger of a medium-sized automobile diesel engine is examined.

A schematic sketch of the turbocharger turbine is depicted in Fig. 2. The rotor consists of a flexible shaft, at which the compressor and the turbine wheel are fixed. The rotor is supported in two identical full-floating ring bearings. Note that the rotor always has some imbalance due to the manufacturing process.

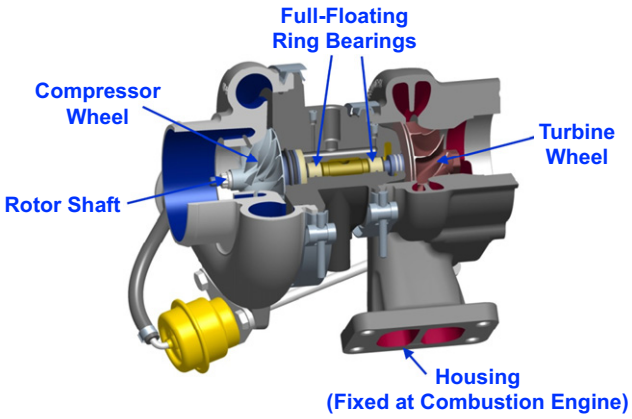

Fig. 1. Automotive Turbocharger.

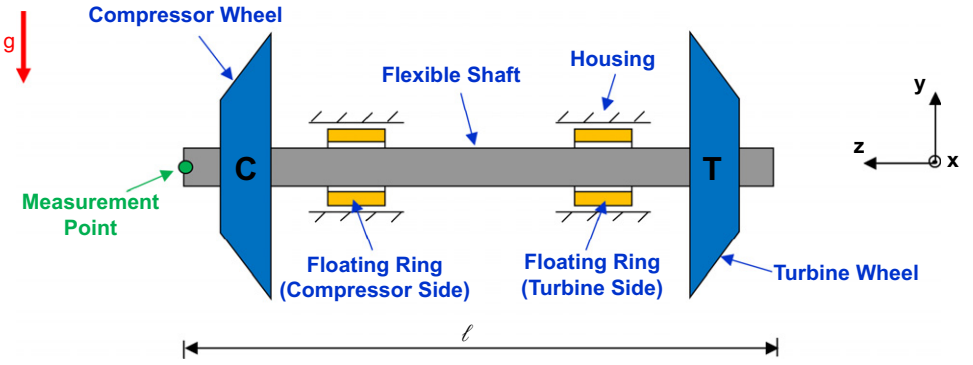

Fig. 2. Schematic sketch of the rotor/bearing system of a turbocharger.

Some data concerning the rotor design and the operating conditions are listed below:

Rotor length	$l \approx 100\,\text{mm}$
Rotor mass (including wheels)	$m \approx 0.1\,\text{kg}$
Ring inner/outer diameter	$D_\text{i} \approx 6.0\,\text{mm} / D_\text{o} \approx 9.5\,\text{mm}$
Ring inner/outer width	$B_\text{i} \approx 3.6\,\text{mm} / B_\text{o} \approx 6.1\,\text{mm}$
Nominal (estimated) imbalance at turbine/compressor wheel	$U_\text{T} \approx 0.1\,\text{g mm} / U_\text{C} \approx 0.05\,\text{g mm}$
Considered rotor speed range	$0 \leqslant \omega_\text{Rotor} \leqslant \approx 162\,000$ rev/min
Oil viscosity (at 20 °C)	$\eta \approx 0.17\,\text{Ns/m}^2$
Oil supply pressure	p_sup (is varied, see below)
Oil supply temperature	T_sup (is varied, see below)

The maximum operating speed of the examined turbocharger is $\omega_\text{Rotor,max} \approx 200\,000$ rev/min. In operation, i.e., during a car drive, the oil supply pressure may fluctuate between $p_\text{sup,min} \approx 0.8$ bar and $p_\text{sup,max} \approx 4.0$ bar; the mean oil supply temperature is $T_\text{sup,mean} \approx 90\,^\circ\text{C}$. In the measurements presented in Section 3, the oil supply pressure p_sup and the oil supply temperature T_sup have been changed. Also, in some test runs an artificial imbalance $U_\text{C,additional}$ has been fixed at the compressor wheel. p_sup and T_sup have been varied in Measurements 1–4 according to realistic parameter changes occurring during the operation (car drive). The imbalance of turbochargers is often unknown or may (significantly) change during operation. In order to get an idea of the sensitivity of imbalance chances, the nominal imbalance has been increased in two steps by applying an artificial imbalance ($U_\text{C,additional} = 0.25\,\text{g mm}$ and $U_\text{C,additional} = 0.57\,\text{g mm}$) at the compressor wheel.

To get a closer insight into the dynamic effects and in order to interpret the measured rotor vibrations, it is useful to have some information about the approximate natural frequencies and natural mode shapes of the turbocharger. For this reason, a linear model of the rotor/bearing system has been created in order to perform a gyroscopic eigenfrequency analysis. The flexible rotor (consisting of rotor shaft, compressor and turbine wheel) shows approximately a linear elastic behavior. The point is to linearize the floating ring bearings, which have a highly nonlinear characteristic. To keep the calculation concise, each floating ring bearing is just replaced by two linear springs (assumed constant spring stiffness $c_x = c_y = 1000\,\text{N/mm}$) acting in the x- and in y-direction. Damping effects have not been considered in the eigenvalue calculation.

A gyroscopic eigenvalue analysis for the turbocharger rotor shows the following results:

- The first two natural modes are (almost) rigid body conical modes (elastic shaft bending is small): the first mode is the *gyroscopic conical reverse mode*; the second mode is the corresponding *gyroscopic conical forward mode*.
- The third and fourth natural modes are approximately rigid body translational modes (elastic shaft bending is little larger compared with the conical modes): the third mode is the *gyroscopic translational reverse mode*; the fourth mode is the corresponding *gyroscopic translational forward mode*.

- The fifth mode is the *first torsional mode*, which is not affected by gyroscopic effects.
- The sixth and seventh natural modes are elastic bending modes: the sixth mode is the *gyroscopic bending reverse mode*; the seventh mode is the corresponding *gyroscopic bending forward mode*.
- All modes—with the exception of the torsional mode—are spherical modes.

The gyroscopic natural frequencies of the turbine at a rotor speed of 135 000 rev/min are:

Mode 1 (conical reverse)	150 Hz
Mode 2 (conical forward)	320 Hz
Mode 3 (translational reverse)	550 Hz
Mode 4 (translational forward)	620 Hz
Mode 5 (torsional)	1910 Hz
Mode 6 (bending reverse)	1500 Hz
Mode 7 (bending forward)	2840 Hz

The mode shapes of the first seven gyroscopic natural modes are depicted in Fig. 3. The development of the eigenfrequencies of these seven modes with increasing rotor speed is shown in Fig. 4.

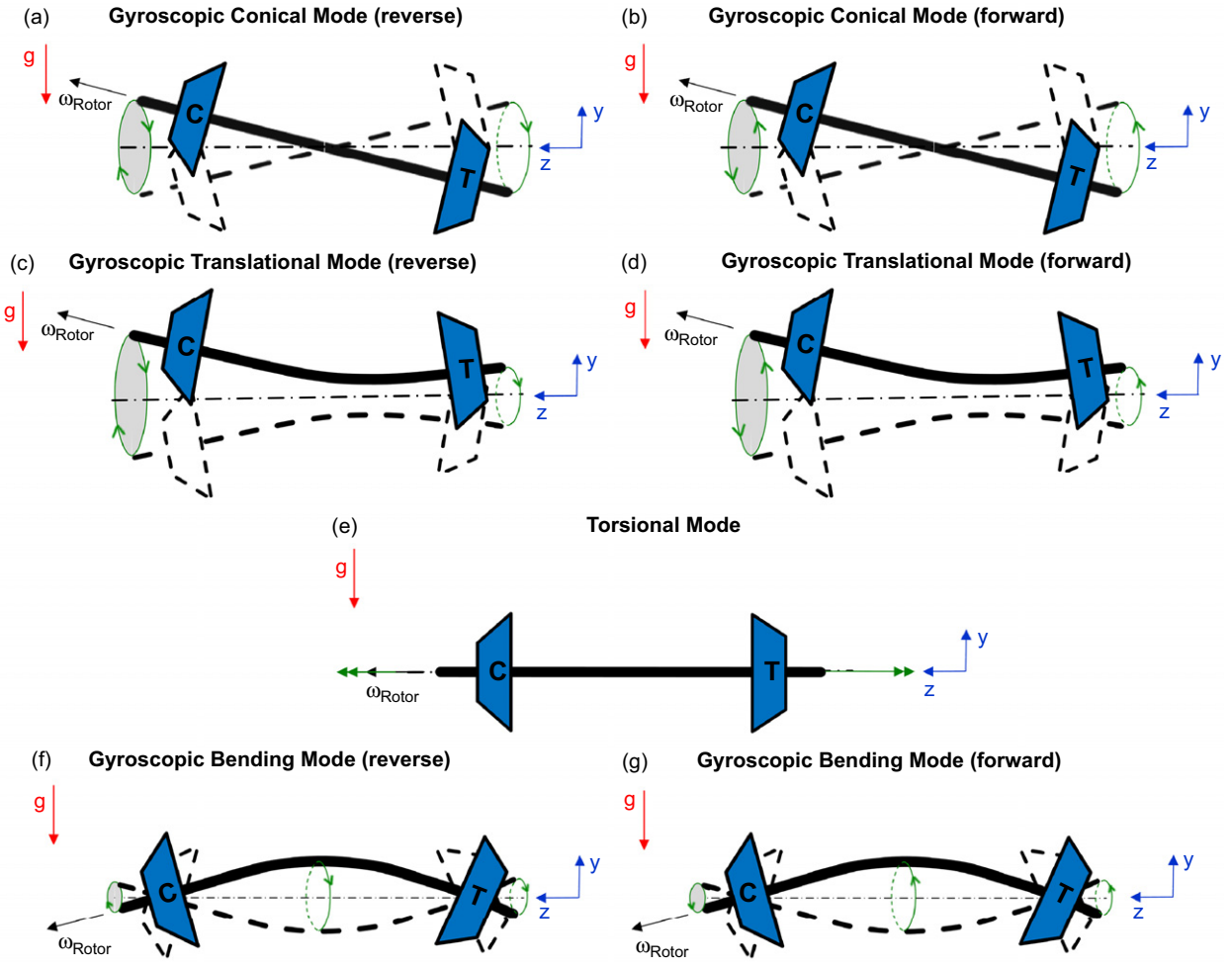

Fig. 3. Gyroscopic mode shapes of the turbocharger rotor in linear bearings for a rotor speed of $\omega_{\mathrm{Rotor}} = 135\,000$ rev/min: (a)–(g) gyroscopic reverse (backward) and forward mode shapes.

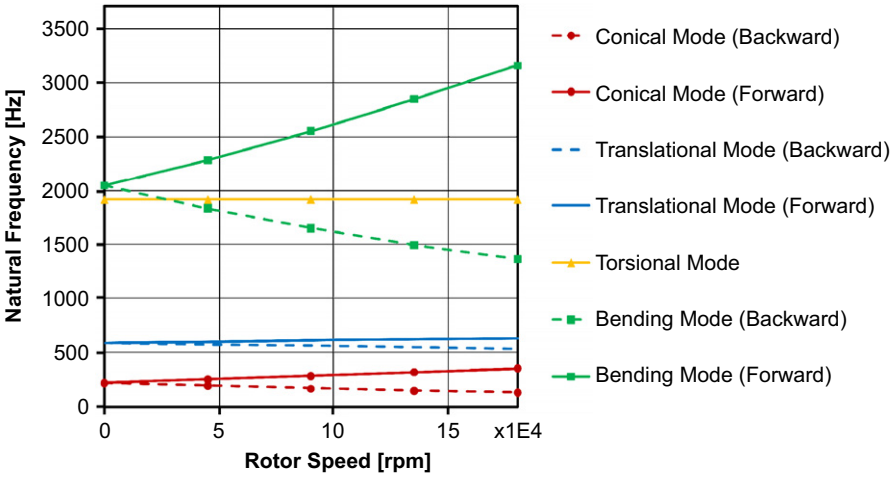

Fig. 4. Gyroscopic natural frequencies of the turbocharger rotor in linear bearings over the rotor speed.

3. Run-up measurements

In this section, test results of turbocharger run-ups are presented and discussed. The measurements were carried out on a *hot-gas turbocharger test rig*. The horizontal and vertical vibrations (x- and y-displacement) of the compressor-sided shaft extension (green measurement point in Fig. 2) were measured with eddy current sensors. The set-up of the hot-gas test rig is depicted in Fig. 5. The turbine wheel is driven by hot gas (inlet temperature $T_{T,inlet} \approx 90\,^{\circ}C$, inlet pressure $p_{T,inlet} \approx 3.5$ bar, outlet temperature $T_{T,outlet} \approx 5\,^{\circ}C$, outlet pressure $p_{T,outlet} \approx 1.1$ bar, mass flow $q_T \approx 0.18$ kg/s). The compressor wheel compresses ambient air (inlet temperature $T_{C,inlet} \approx 22\,^{\circ}C$, inlet pressure $p_{C,inlet} \approx 0.95$ bar, outlet temperature $T_{C,outlet} \approx 130\,^{\circ}C$, outlet pressure $p_{C,outlet} \approx 2.1$ bar, mass flow $q_C \approx 0.13$ kg/s). The measurements start at a rotor speed of 0 rev/min. To accelerate the rotor up to the top speed of $\approx 162\,000$ rev/min, the hot-gas flow at the turbine is continuously increased.

Six test runs with different operating conditions have been carried out. The oil supply pressure p_{sup} as well as the oil supply temperature T_{sup} were changed. Furthermore, an additional imbalance $U_{C,additional}$ has been fixed at the compressor wheel. The operating conditions for the six run-up measurements are summarized in Table 1. The time series signals of the measured lateral vibrations (x,y-displacement) of the measurement point have been prepared by a *fast Fourier analysis* (*FFT*). The corresponding frequency spectra are depicted in Figs. 6–11. The system response is dominated by four main frequencies:

(i) The *Synchronous* (due to rotor imbalance),
(ii) The *1. Subsynchronous* (*oil whirl/whip* of the inner oil films excites the *gyroscopic conical forward mode*),
(iii) The *2. Subsynchronous* (*oil whirl/whip* of the inner oil films excites the *gyroscopic translational forward mode*),
(iv) The *3. Subsynchronous* (*oil whirl/whip* of the outer oil films excites the *gyroscopic conical forward mode*).

The other frequencies observed in the frequency spectra are superharmonics, subharmonics and combination frequencies of the four main frequencies. Fig. 12 shows again the frequency spectrum for Measurement 2 (Fig. 7(a)) and explains in detail the occurring frequencies. It means:

- *Syn* = *Synchronous*,
- *Sub1* = *1. Subsynchronous*,
- *Sub2* = *2. Subsynchronous*,
- *Sub3* = *3. Subsynchronous*.

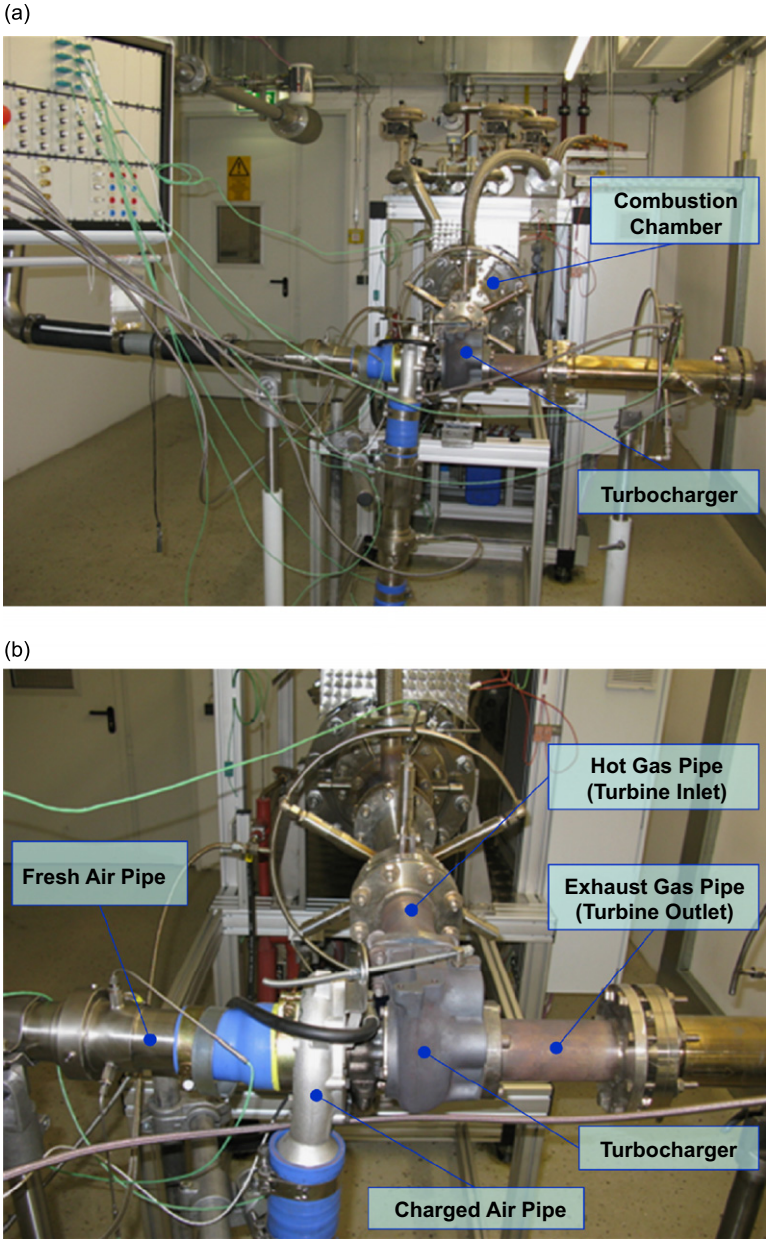

Fig. 5. Set-up of hot-gas turbocharger test rig.

Table 1
Operating conditions for run-up measurements.

	P_{sup} (bar)	T_{sup} (°C)	$U_{C,additional}$ (g mm)
Measurement 1	3	75	–
Measurement 2	1.5	75	–
Measurement 3	3	90	–
Measurement 4	1.5	90	–
Measurement 5	3	75	0.25
Measurement 6	3	75	0.57

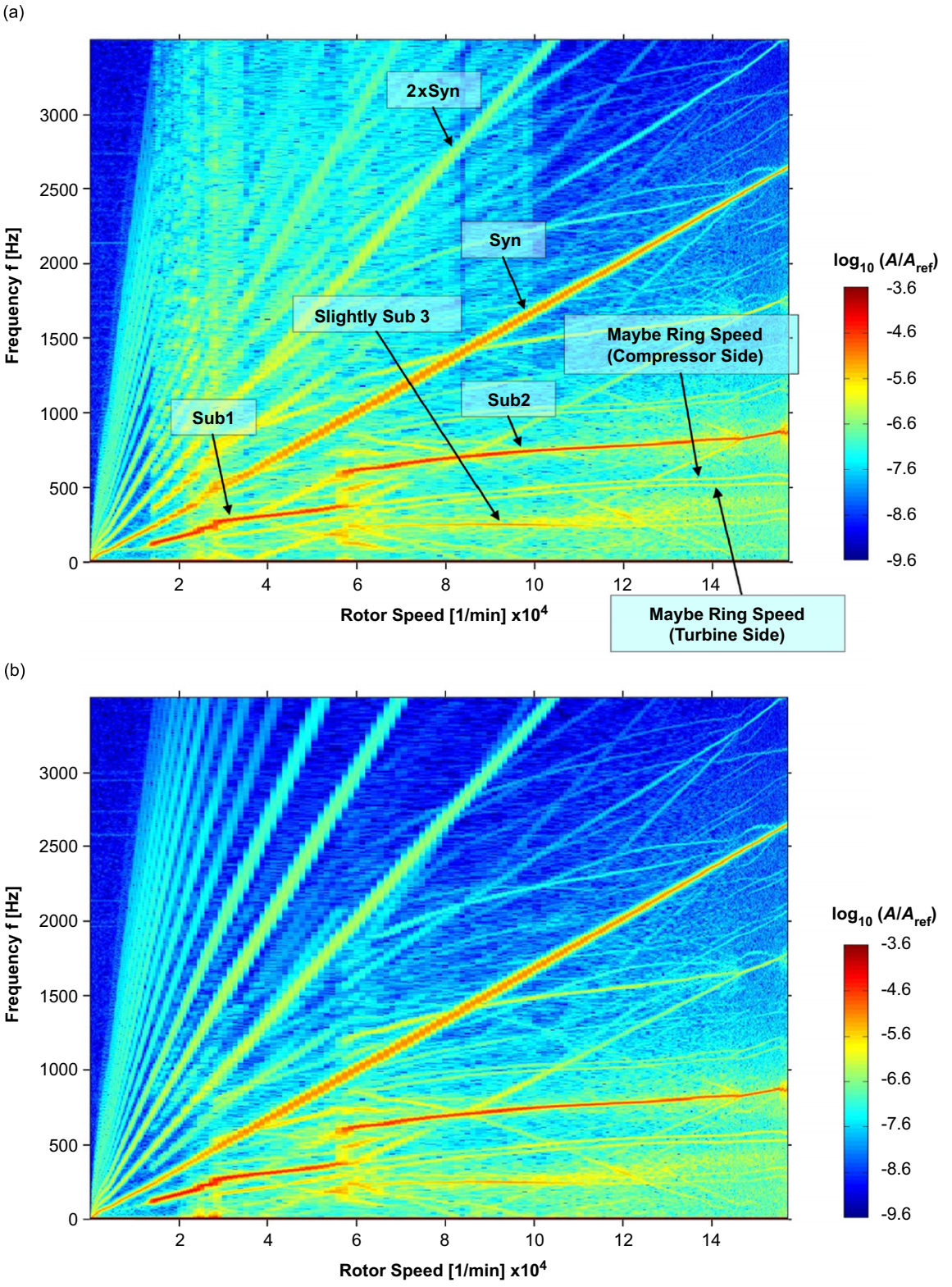

Fig. 6. Frequency spectra of Measurement 1; $p_{sup} = 3$ bar; $T_{sup} = 75\,^{\circ}$C; (a) x-displacement; (b) y-displacement.

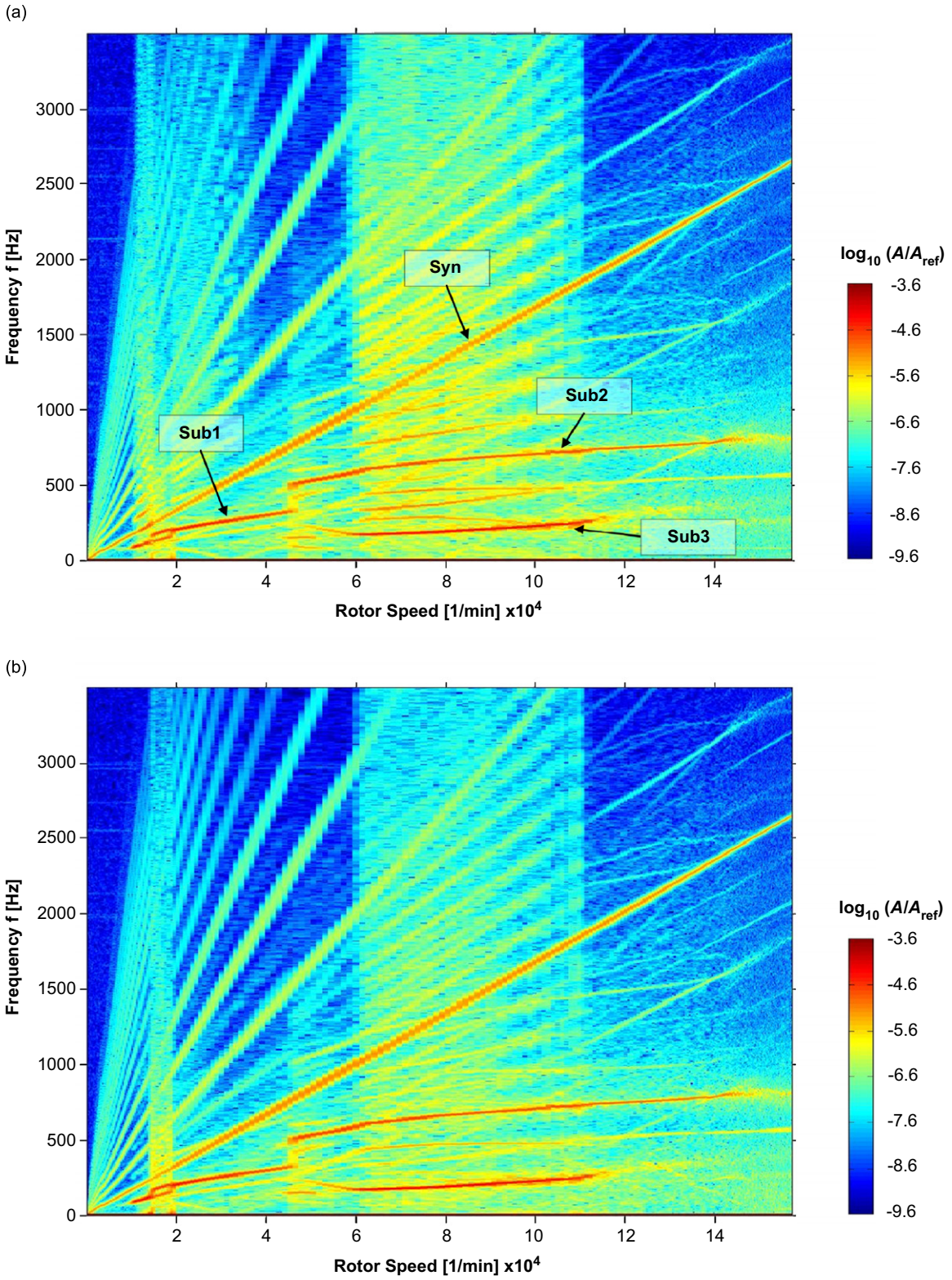

Fig. 7. Frequency spectra of Measurement 2; $p_{sup} = 1.5$ bar; $T_{sup} = 75\,^{\circ}$C; (a) x-displacement; (b) y-displacement.

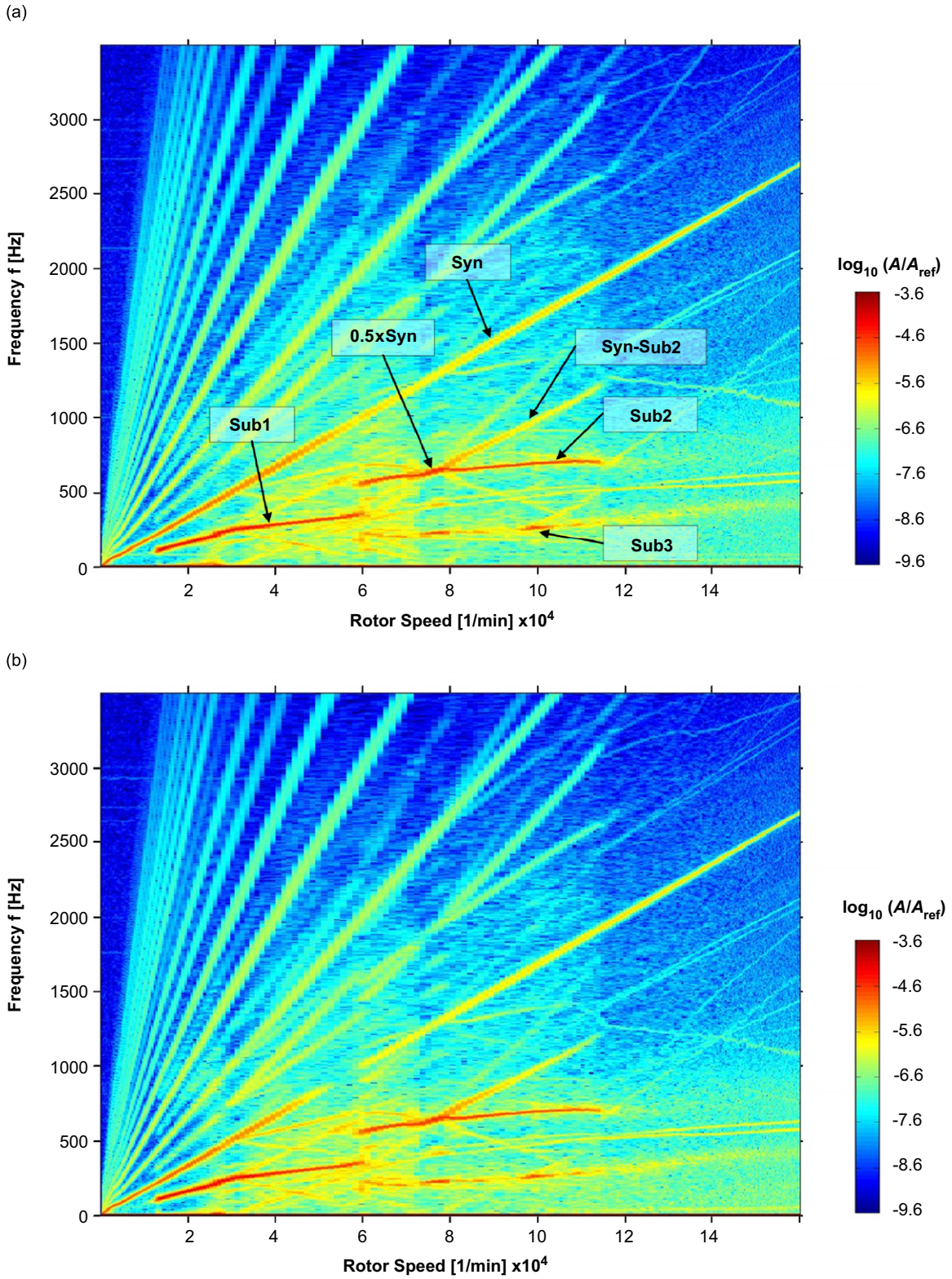

Fig. 8. Frequency spectra of Measurement 3, $p_{sup} = 3$ bar; $T_{sup} = 90\,^{\circ}$C; (a) x-displacement; (b) y-displacement.

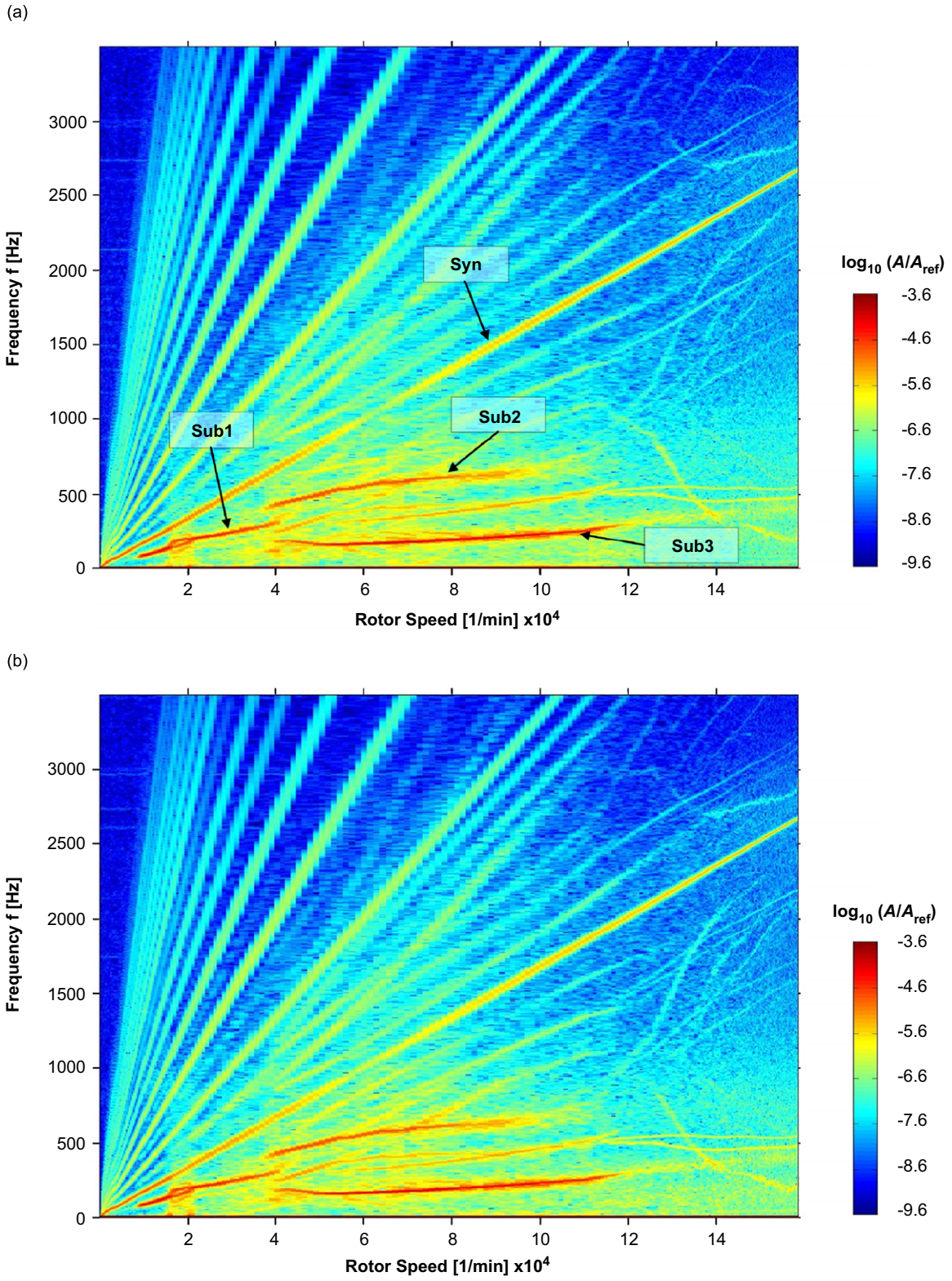

Fig. 9. Frequency spectra of Measurement 4; $p_{sup} = 1.5$ bar; $T_{sup} = 90\,^{\circ}$C; (a) x-displacement; (b) y-displacement.

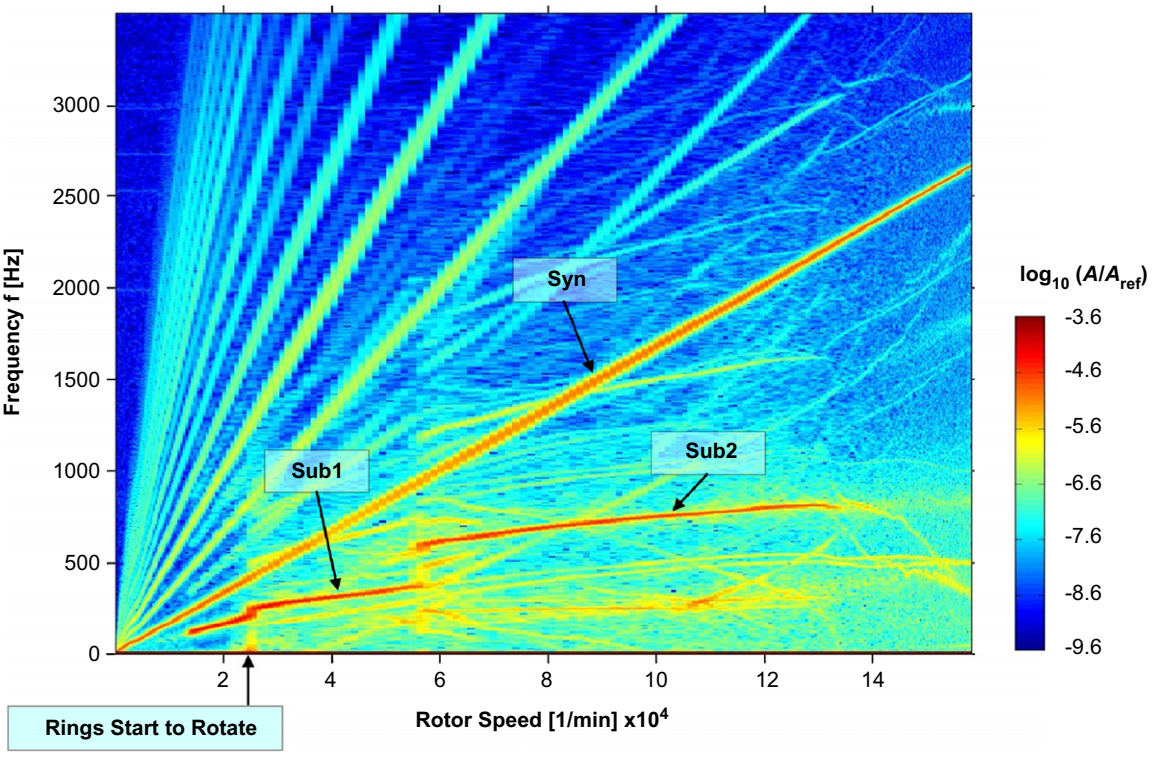

Fig. 10. Frequency spectrum of Measurement 5; $p_{sup} = 3$ bar; $T_{sup} = 75\,^{\circ}$C; additional imbalance: $U_{C,additional} = 0.25$ g mm.

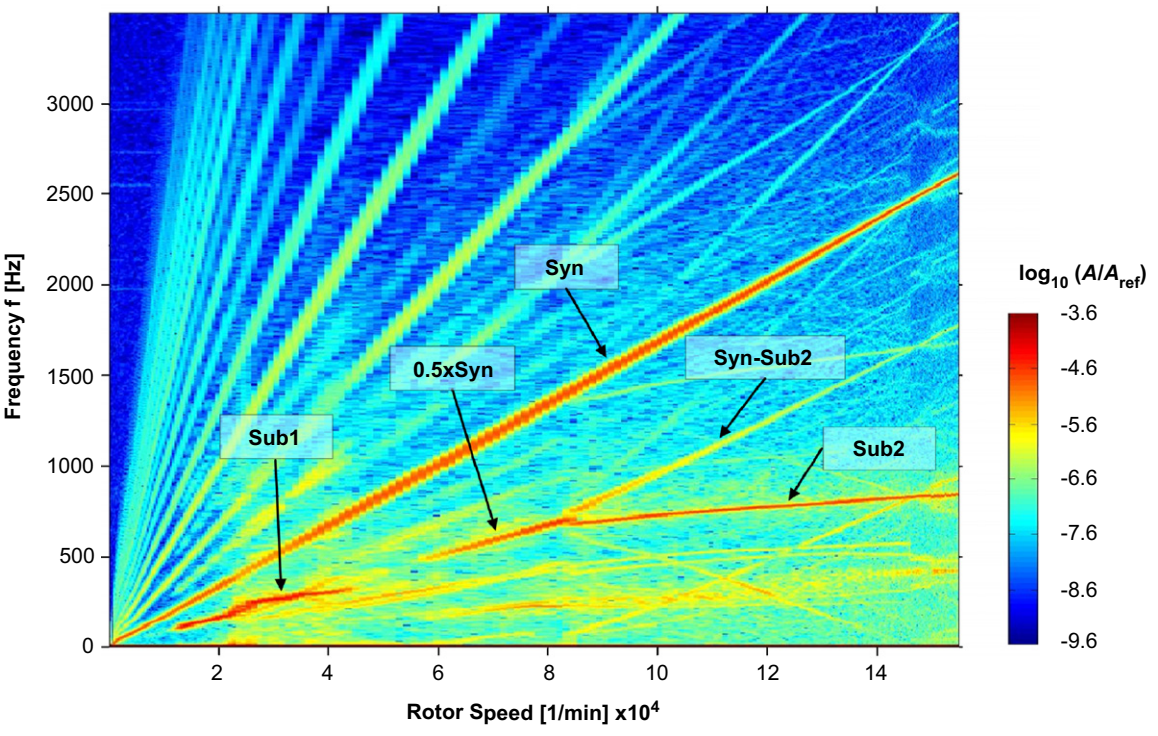

Fig. 11. Frequency spectrum of Measurement 6; $p_{sup} = 3$ bar; $T_{sup} = 75\,^{\circ}$C; additional imbalance: $U_{C,additional} = 0.57$ g mm.

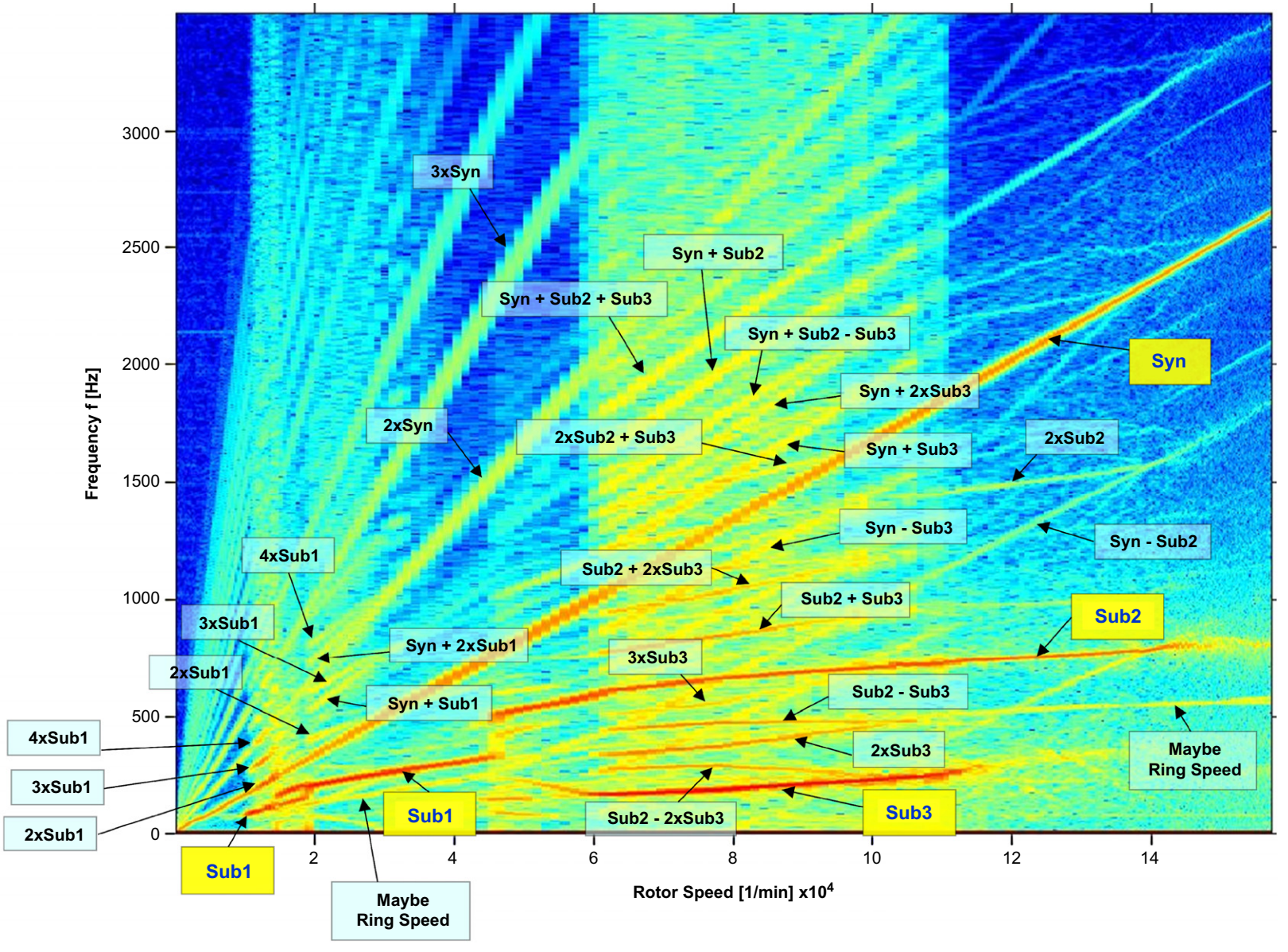

Fig. 12. Frequency spectrum of Measurement 2 (x-displacement of measurement point); detailed analysis of occurring vibration frequencies.

Turbocharger run-up simulations (see Appendix A.3) "prove" the claims (ii)–(iv), namely that—very roughly speaking—the inner and outer *oil whirl/whip* can be considered as "externally applied motions", exciting the rotor with the corresponding *whirl/whip* frequency. It depends on the actual *whirl/whip* frequency, which natural mode is excited. The inner fluid films usually become unstable already at low rotor speeds, first exciting the *gyroscopic conical forward mode* and later the *gyroscopic translational forward mode*. At higher rotor speeds, the outer fluid films may also become unstable (possibly simultaneously with the inner oil films) and excite the *gyroscopic conical forward mode*. The simultaneous occurrence of the inner and outer *whirl/whip* can clearly be seen in Figs. 7 and 9.

The mode shapes calculated in Section 2 were accomplished, assuming a constant bearing stiffness ($c_x = c_y = 1000\,\mathrm{N/mm}$) over the whole speed range (see Fig. 4). Since the characteristic of the floating ring bearings is highly nonlinear and changes with increasing rotor speed, the calculated gyroscopic eigenfrequencies in Fig. 4 may be considered qualitatively rather than quantitatively. We also neglected damping in the eigenvalue analyses (if damping is moderate, the mode shapes and natural frequencies are only slightly influenced by damping). Note that the damping behavior of the fluid films also changes with increasing rotor speed. Despite the simplifications and assumptions used for the eigenvalue analysis, the measured and simulated subsynchronous frequencies (*1.*, *2.* and *3. Subsynchronous*) can clearly be related to the calculated gyroscopic natural modes (Figs. 3 and 4), which are excited by the inner and outer *oil whirl/whip*.

Next, the measured frequency spectra are discussed and interpreted, see Figs. 6–12. It should be stressed that we used a logarithmic scale for the normalized vibration amplitudes. We apologize for not supplying the reference amplitude A_{ref}.

Measurement 1 (Fig. 6): Frequency spectra of the x- and y-displacement of the measurement point are shown in Fig. 6. Both plots are very similar.

- Up to $\omega_{\mathrm{Rotor}} \approx 1.3\mathrm{E}4[1/\mathrm{min}]$, the rotor performs stable imbalance vibrations around a stable equilibrium position. The dominating frequency is the imbalance vibration (*Synchronous*). Also, some superharmonic frequencies ($2\times$ *Synchronous*, $3\times$ *Synchronous, etc.*) are observed.
- At $\omega_{\mathrm{Rotor}} \approx 1.3\mathrm{E}4[1/\mathrm{min}]$, the inner fluid films become unstable and excite the *gyroscopic conical forward mode* (*1. Subsynchronous*). In the range $\approx 1.3\mathrm{E}4[1/\mathrm{min}] \leqslant \omega_{\mathrm{Rotor}} \leqslant \approx 5.7\mathrm{E}4[1/\mathrm{min}]$, the transition from *oil whirl* to *oil whip* takes place (see also Appendix A.1). Provided that the ring rotates, the nominal *whirl* frequency of the inner oil film is approximately given by $\omega_{\mathrm{sub\_i,nominal}} \approx 0.5 \cdot (\omega_{\mathrm{Rotor}} + \omega_{\mathrm{Ring}})$. One detects that the ratio $\omega_{\mathrm{sub1}}/\omega_{\mathrm{sub\_i,nominal}}$ successively decreases with increasing rotor speed, which indicates the transition from *oil whirl* to *oil whip*.
- At $\omega_{\mathrm{Rotor}} \approx 5.7\mathrm{E}4[1/\mathrm{min}]$, a jump phenomenon is observed. The inner fluid films remain unstable, but the *oil whirl/whip* of the inner fluid films now excites the *gyroscopic translational forward mode*. This frequency is called *2. Subsynchronous* and remains up to the maximum rotor speed. Again, one can clearly detect the transition from *oil whirl* to *oil whip*.
- The *3. Subsynchronous* (*oil whirl/whip* of unstable outer fluid films excites the *gyroscopic conical forward mode*) only slightly occurs in the frequency spectrum (see spectrum in the range $\approx 8\mathrm{E}4[1/\mathrm{min}] \leqslant \omega_{\mathrm{Rotor}} \leqslant \approx 10\mathrm{E}4[1/\mathrm{min}]$).

Measurement 2 (Fig. 7): In contrast to Measurement 1, the oil supply pressure p_{sup} is reduced from 3 to 1.5 bar. In comparison to Measurement 1, one observes that the onset of *1. Subsynchronous* and especially the onset of *2. Subsynchronous* occurs earlier in the frequency spectrum. Furthermore, the spectrum clearly shows the *3. Subsynchronous*.

Measurement 3 (Fig. 8): Compared to Measurement 1, the oil supply temperature T_{sup} is increased from 75 to 90 °C. In comparison to Measurement 1, one detects that the *2. Subsynchronous* is passed through so that at higher rotor speeds the rotor (the fluid films) becomes stable again and only performs imbalance vibrations around a stable equilibrium position.

Measurement 4 (Fig. 9): In contrast to Measurement 1, the oil supply pressure p_{sup} is reduced from 3 to 1.5 bar and the oil supply temperature T_{sup} is increased from 75 to 90 °C. In comparison with Measurement 2, the jump from the *1. Subsynchronous* to the *2. Subsynchronous* (*3. Subsynchronous*) occurs earlier. Also, the *2. Subsynchronous* is even faster passed through than in Measurement 3.

Measurement 5 (Fig. 10): Compared to Measurement 1, an additional imbalance of $U_{C,additional} = 0.25$ g mm is fixed at the compressor wheel. The spectrum is very similar to Measurement 1. One difference is that the *2. Subsynchronous* is passed through. As expected, the amplitude of the *Synchronous* is larger.

Measurement 6 (Fig. 11): In comparison with Measurement 1, an additional imbalance of $U_{C,additional} = 0.57$ g mm is fixed at the compressor wheel. Compared to Measurement 5, the amplitude of the *Synchronous* is further increased. The spectrum shows two interesting effects.

In the speed range $\approx 4.4E4[1/min] \leqslant \omega_{Rotor} \leqslant \approx 5.8E4[1/min]$, the system becomes intermittently stable. The reason for the intermittent stabilization is most likely that the increased imbalance entails higher bearing forces, which stabilizes the rotor (a similar effect for a rotor supported in single oil film bearings is, e.g., reported in Ref. [15]).

A remarkable effect can further be observed in the speed range $\approx 5.8E4[1/min] \leqslant \omega_{Rotor} \leqslant \approx 8.4E4[1/min]$, where the spectrum exhibits a subsynchronous frequency of exactly $1/2 \cdot \omega_{Rotor}$ with large amplitude. The $1/2 \cdot \omega_{Rotor}$ frequency may be explained as follows: Due to system nonlinearities, primarily introduced by the bearings, the system is generally able to generate "conventional" supersynchronous frequencies $n \cdot \omega_{Rotor}$ ($n = 1,2,3,\ldots$) and subsynchronous frequencies $m \cdot \omega_{Rotor}$ ($m = 1/2,\ 1/3,\ 1/4,\ldots$), see for instance Refs. [19,21]. At $\omega_{Rotor} \approx 5.8E4[1/min]$, the inner fluid films become unstable again (intermittent stabilization is finished). At this point, the corresponding *oil whirl/whip* frequency is obviously close to the subsynchronous $1/2 \cdot \omega_{Rotor}$ and the *oil whirl/whip* frequency locks at $1/2 \cdot \omega_{Rotor}$. The frequency locking remains up to $\omega_{Rotor} \approx 8.4E4[1/min]$. Hence, we observe the astonishing phenomenon that a limit cycle (inner *oil whirl/whip*) is locking at a subsynchronous frequency ($1/2 \cdot \omega_{Rotor}$). Note that the above described locking (synchronization) effect is also detected in Measurement 3 (Fig. 8) in the range $\approx 7.4E4[1/min] \leqslant \omega_{Rotor} \leqslant \approx 7.8E4[1/min]$. Locking phenomena in connection with self-excited systems, which are externally excited, are well-known in literature. For instance, the externally excited Van-der-Pol oscillator exhibits frequency locking [19].

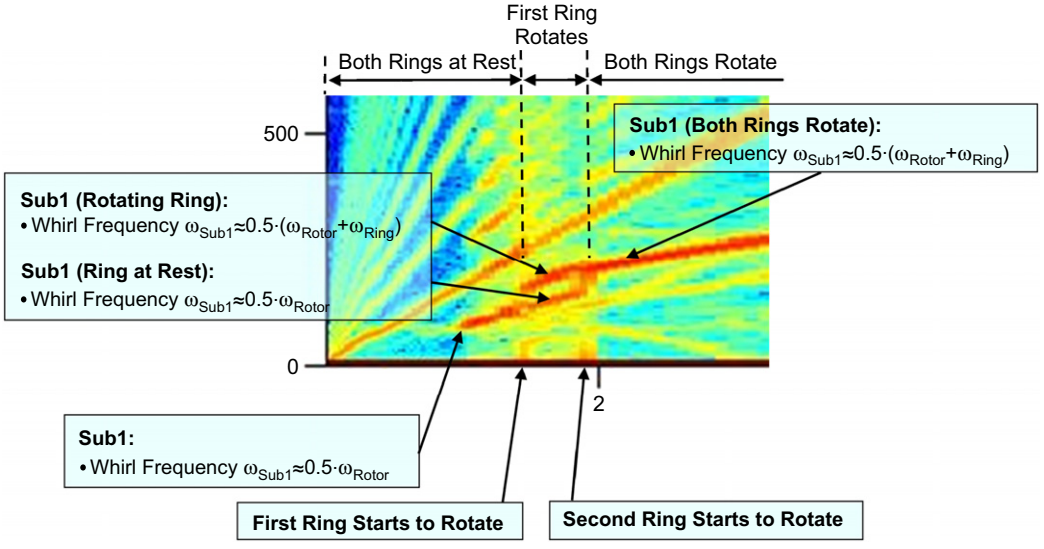

Fig. 13. Detail illustrating state of both rings.

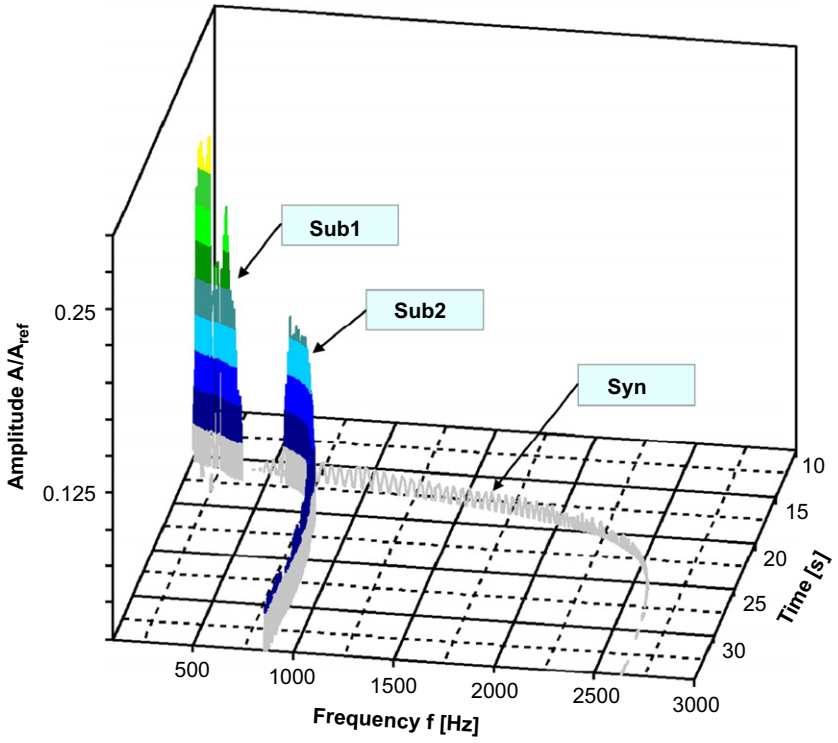

Fig. 14. 3D-waterfall diagram of Measurement 1; $p_{sup} = 3$ bar; $T_{sup} = 75\,^{\circ}$C; y-displacement.

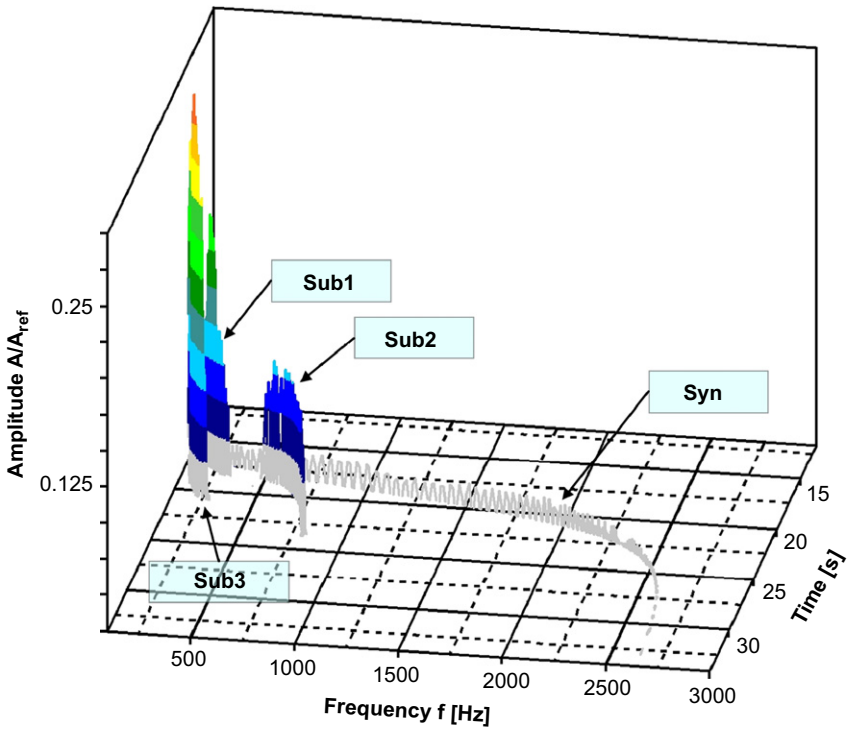

Fig. 15. 3D-waterfall diagram of Measurement 2; $p_{sup} = 1.5$ bar; $T_{sup} = 75\,^{\circ}$C; y-displacement.

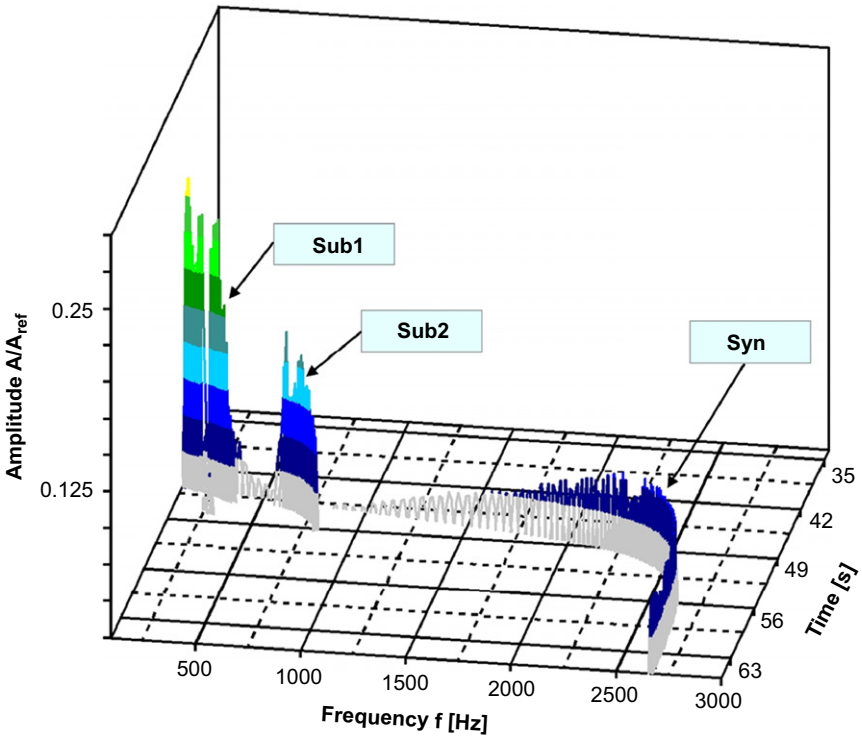

Fig. 16. 3D-waterfall diagram of Measurement 5, $p_{sup} = 3$ bar, $T_{sup} = 75\,^{\circ}$C, additional imbalance: $U_{C,additional} = 0.25$ g mm; y-displacement.

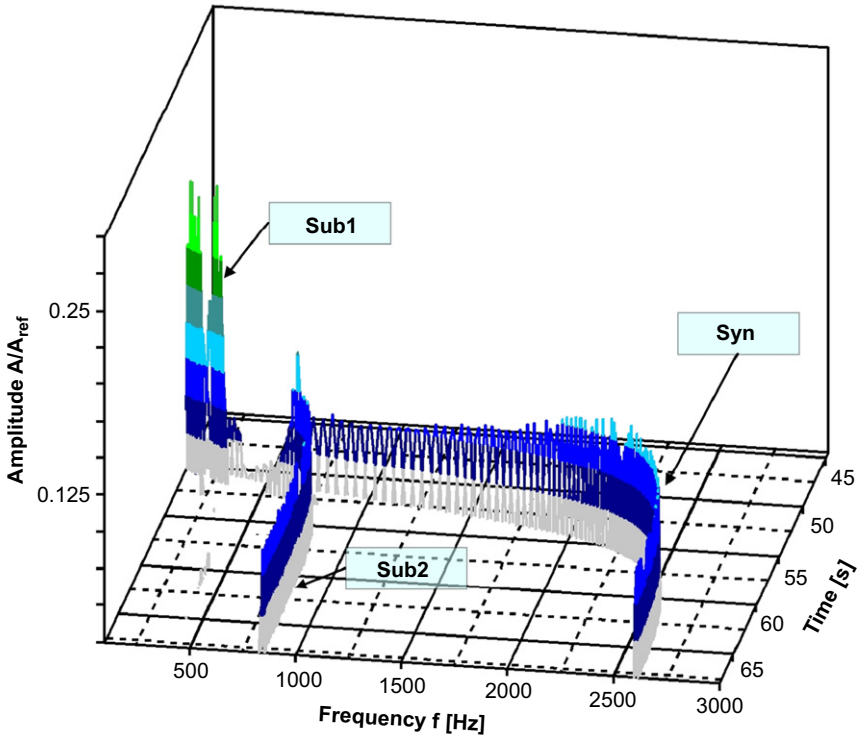

Fig. 17. 3D-waterfall diagram of Measurement 6, $p_{sup} = 3$ bar, $T_{sup} = 75\,^{\circ}$C; additional imbalance $U_{C,additional} = 0.57$ g mm; y-displacement.

Fig. 13 shows a detail of Fig. 12 and illustrates the different times, where the two rings start to rotate. Starting the run-up with zero rotor speed ($\omega_{\mathrm{Rotor}}=0$), it is known from test runs, where ring speeds have been directly measured, that the floating rings usually do not rotate at low rotor speeds due to dry friction between ring and housing. If the friction torque in the inner oil film is large enough, the ring starts to rotate. It is also known from direct ring measurements that if the ring once rotates, it will normally not come to rest again, when the rotor speed is steadily increased. For $\omega_{\mathrm{Rotor}}<\approx 1.0\mathrm{E}4[1/\mathrm{min}]$, the rotor only performs imbalance vibrations (*Synchronous*). At $\omega_{\mathrm{Rotor}}\approx 1.0\mathrm{E}4[1/\mathrm{min}]$, both inner fluid films (compressor-sided and turbine-sided) become unstable and the *1. Subsynchronous* appears. The whirl frequency is $\approx 0.5\cdot\omega_{\mathrm{Rotor}}$. Note: The nominal inner *oil whirl* frequency is $\approx 0.5\cdot\omega_{\mathrm{Rotor}}$ for the case that the ring does not rotate and $\approx 0.5\cdot(\omega_{\mathrm{Rotor}}+\omega_{\mathrm{Ring}})$ for the case that the ring does rotate [10,26]. Hence, up to $\omega_{\mathrm{Rotor}}\approx 1.4\mathrm{E}4[1/\mathrm{min}]$ neither the compressor-sided nor the turbine-sided ring rotates. At $\omega_{\mathrm{Rotor}}\approx 1.4\mathrm{E}4[1/\mathrm{min}]$, the first ring starts to rotate so that one ring is at rest and the other ring rotates. As a consequence, one observes two *whirl* frequencies: The inner fluid film of the bearing, where the ring rotates, generates a *whirl* frequency of $\approx 0.5\cdot(\omega_{\mathrm{Rotor}}+\omega_{\mathrm{Ring}})$, while the inner fluid film of the bearing, where the ring does not rotate, generates a *whirl* frequency of $\approx 0.5\cdot\omega_{\mathrm{Rotor}}$. At $\omega_{\mathrm{Rotor}}\approx 1.9\mathrm{E}4[1/\mathrm{min}]$, the second ring also starts to rotate and one observes only one *whirl* with a frequency of $\approx 0.5\cdot(\omega_{\mathrm{Rotor}}+\omega_{\mathrm{Ring}})$. In Measurement 2, the two rings start to rotate at different times. This is not mandatory: In Measurement 5, for instance, both rings start to rotate simultaneously.

3D waterfall diagrams for the Measurements 1, 2, 5, 6 (y-displacement of measuring point) can be seen in Figs. 14–17. In addition to the 2D spectra, the 3D waterfall diagrams also contain the time information. As can be seen, the run-ups are performed in $\Delta t\approx 15\,\mathrm{s}$ (speed increase is not uniform). Please note that—in contrast to the 2D spectra—a linear scale has been used. Again, we apologize for not providing the reference amplitude A_{ref}. It should be mentioned that amplitudes $A\leqslant 0.025\cdot A_{\mathrm{ref}}$ have been cutoff in the 3D plots so that the plots only show the main frequencies (Syn, Sub1, Sub2 and Sub3).

Remark about the measured oil outlet temperatures: The measured mean oil outlet temperature (mixing temperature of both floating ring bearings and the axial bearing) was $T_{\mathrm{out}}\approx 90\,^{\circ}\mathrm{C}$ for the case $T_{\mathrm{sup}}\approx 75\,^{\circ}\mathrm{C}$. It should be mentioned that T_{out} only increased slightly during the run-up measurement: $T_{\mathrm{out}}\approx 88\,^{\circ}\mathrm{C}$ at the beginning of the run-up and $T_{\mathrm{out}}\approx 92\,^{\circ}\mathrm{C}$ at the end of the run-up. In the case of higher oil supply temperature $T_{\mathrm{sup}}\approx 90\,^{\circ}\mathrm{C}$, the mean oil outlet temperature was $T_{\mathrm{out}}\approx 108\,^{\circ}\mathrm{C}$ (the outlet temperature also changed only slightly during the run-up).

4. Conclusions

Measured rotor vibrations of an automotive turbocharger rotor were presented and the occurring dynamic effects explained. The main excited natural modes of the rotor/bearing system are the *gyroscopic conical forward mode* and the *gyroscopic translational forward mode*, both almost rigid body modes with slight bending. The measurements show that the system exhibits four main frequencies. The first main frequency is the synchronous vibration (*Synchronous*) due to rotor imbalance. The second dominating frequency is generated by the *oil whirl/whip* of the inner fluid films, which excite the *gyroscopic conical forward mode* (*1. Subsynchronous*). The third main frequency is also caused by the *oil whirl/whip* of the inner films, which now excite the *gyroscopic translational forward mode* (*2. Subsynchronous*). The fourth main frequency is generated by the *oil whirl/whip* of the outer fluid films, which excite the *gyroscopic conical forward mode* (*3. Subsynchronous*). Superharmonics, subharmonics and combination frequencies—created by the four main frequencies—generate the other frequencies, which can be seen in the frequency spectra.

The influence of different operating conditions on the rotor vibrations was examined. Decreasing the oil supply pressure favors the occurrence of the *3. Subsynchronous*. Also, the jump from the *1. Subsynchronous* into the *2. Subsynchronous* (*3. Subsynchronous*) takes place at lower rotor speeds. Increasing the oil supply temperature slightly favors the occurrence of the *3. Subsynchronous*.

Acknowledgments

The support of this work by the Volkswagen AG in Wolfsburg (Germany) is gratefully acknowledged. Special thanks to Dipl.-Ing. Michael Kämpfner for the release of the measurement data.

Appendix A

In a wide speed range, the dynamics of turbocharger rotors in full-floating ring bearings is dominated by *oil whirl/whip* phenomena occurring in the inner and outer fluid films of the floating ring bearings. *Oil whirl/whip* phenomena are self-excited vibrations, induced by the fluid flow in the bearing gap. The mechanical causes for self-excited vibrations are different [19–21]:

- Friction-induced self-excited vibrations.
- Self-excited vibrations due to negative damping (e.g., Van-der-Pol oscillator).
- Flow-induced self-excited vibrations (e.g., flutter instability).
- etc.

In the case of hydrodynamic bearings, the self-excited vibrations are caused by circulatory forces generated by the bearings. Linearizing a rotor/bearing system about a (stable) equilibrium position, one obtains the well-known linear equations of motion $\mathbf{M}\cdot\mathbf{q}+(\mathbf{D}+\mathbf{G})\cdot\mathbf{q}+(\mathbf{K}+\mathbf{N})\cdot\mathbf{q}=\mathbf{f}$ where $\mathbf{M}$ is the mass matrix, $\mathbf{D}$ the symmetric damping matrix, $\mathbf{G}$ the skew-symmetric gyroscopic matrix, $\mathbf{K}$ the symmetric stiffness matrix and $\mathbf{N}$ the skew-symmetric circulatory matrix. Note that the $\mathbf{N}$-matrix is generated by the hydrodynamic bearings [1–3]. $\mathbf{q}$ denotes the generalized coordinates of the rotor/bearing system, collecting rigid body as well as elastic deformation coordinates [22]. $\mathbf{f}$ terms the force vector. The matrices depend on system and operating parameters, especially on the rotor speed ω_{Rotor}. If ω_{Rotor} is continuously increased, the system may become unstable, because the $\mathbf{N}$-matrix more and more dominates the system dynamics with increasing rotor speed. If ω_{Rotor} reaches the threshold of instability ω_{Stab}, the system becomes unstable and reaches the *oil whirl/whip* region.

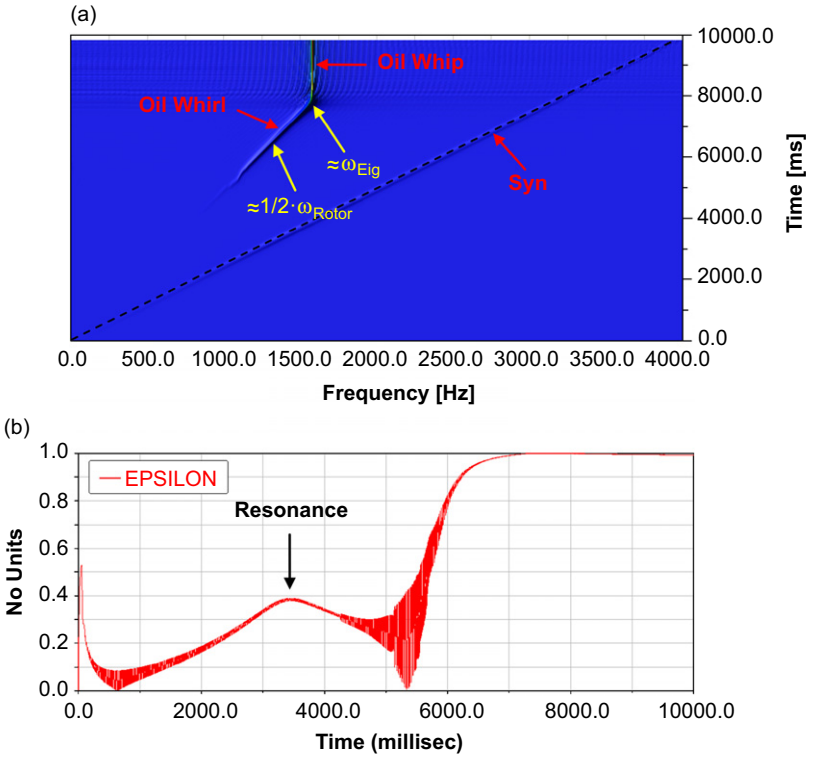

Fig. 18. Run-up simulation of a Jeffcott rotor symmetrically supported in plain hydrodynamic bearings; (a) frequency spectrum of rotor y-displacement; (b) relative bearing eccentricity.

A.1. Run-up simulation of a Jeffcott rotor in plain hydrodynamic bearings

We consider a Jeffcott rotor (mass: $m_{\text{Jeffcott}} = 0.1\,\text{kg}$; bending stiffness: $c_{\text{Shaft}} = 10\,000\,\text{N/mm}$; rotor imbalance: $U_{\text{Jeffcott}} = 0.4\,\text{g mm}$) symmetrically supported in two plain hydrodynamic journal bearings (bearing diameter: $D = 6.0\,\text{mm}$; bearing width: $B = 3.6\,\text{mm}$; relative bearing clearance: $\psi = 3.8\text{E}{-3}$; oil viscosity: $\eta = 1\text{E}{-2}\,\text{Ns/m}^2$). External damping and internal shaft damping is assumed to be small. Fig. 18 depicts the frequency spectrum of the rotor vibrations for a run-up simulation, where rotor speed is linearly increased from 0 up to 4000 Hz in 10 000 ms. For $t \leqslant \approx 5500\,\text{ms}$, rotor amplitudes and bearing eccentricities are comparatively small, except near resonance at $t \approx 3400\,\text{ms}$. At $t \approx 5500\,\text{ms}$, the rotor becomes completely unstable and reaches the *oil whirl* region, where the subsynchronous frequency (*oil whirl* frequency, *half frequency whirl*) locks at $\approx 0.5 \cdot \omega_{\text{Rotor}}$. Further increasing rotor speed, the rotor amplitudes continuously increase. At $t \approx 7900\,\text{ms}$, the rotor reaches the *oil whip* region, where the *whirl* frequency locks at the eigenfrequency of the rotor. The *oil whip* brings the rotor into resonance, so that large rotor amplitudes are observed. For a further discussion on the bifurcation behavior of rotors in hydrodynamic journal bearings, see for instance Refs. [23–25].

A.2. Run-up simulation of a Jeffcott rotor in full-floating ring bearings

Next, we consider a Jeffcott rotor (mass $m_{\text{Jeffcott}} = 0.1\,\text{kg}$; bending stiffness $c_{\text{Shaft}} = 3000\,\text{N/mm}$; rotor imbalance $U_{\text{Jeffcott}} = 0.2\,\text{g mm}$), symmetrically supported in two full-floating ring bearings (inner/outer bearing diameter: $D_i = 6.0\,\text{mm}/D_o = 9.5\,\text{mm}$; inner/outer bearing width: $B_i = 3.6\,\text{mm}/B_o = 6.1\,\text{mm}$; inner/outer relative bearing clearance: $\psi_i = 3.8\text{E}{-3}/\psi_o = 6.7\text{E}{-3}$; inner/outer oil viscosity: $\eta_i \approx 0.01\,\text{Ns/m}^2/\eta_o \approx 0.015\,\text{Ns/m}^2$). The frequency spectrum of the rotor amplitudes is shown in Fig. 19 (run-up simulation from 0–4000 Hz in 10 000 ms). For $t < \approx 1800\,\text{ms}$, the rotor is stable and performs imbalance vibrations around

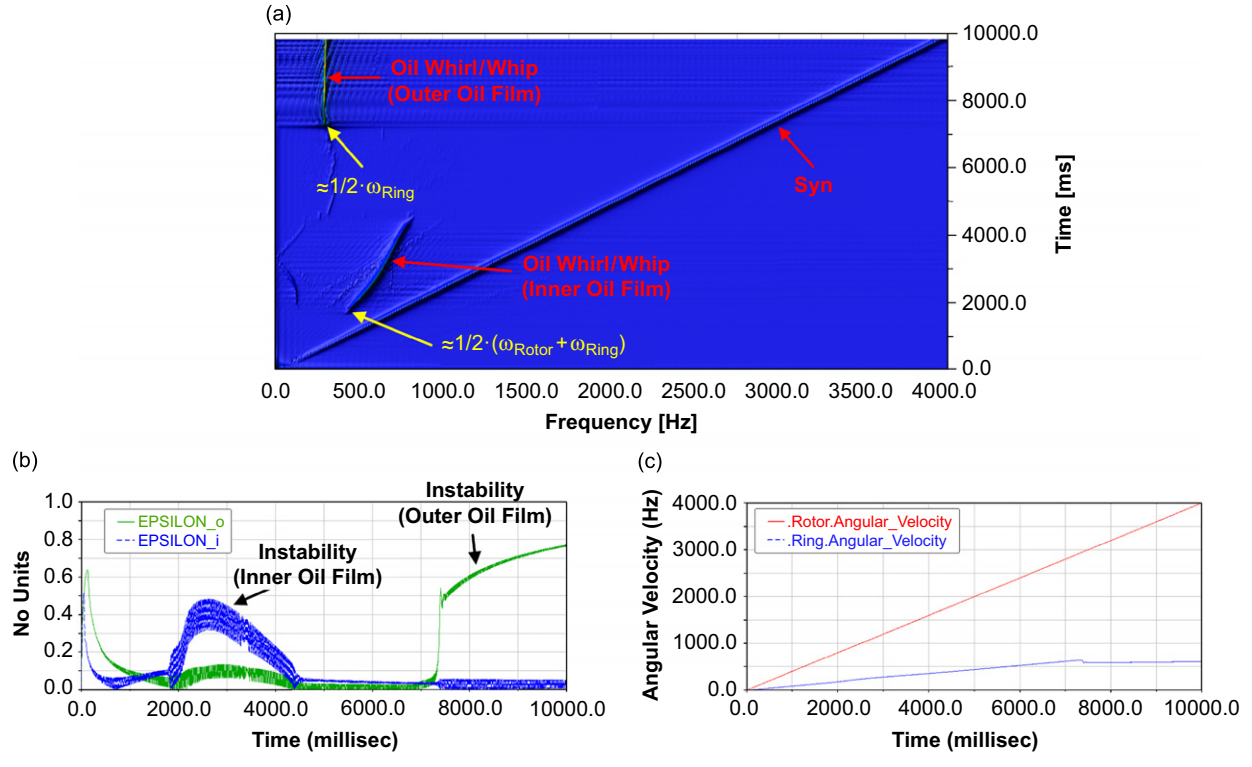

Fig. 19. Run-up simulation of a Jeffcott rotor symmetrically supported in full-floating ring bearings; (a) frequency spectrum of rotor y-displacement; (b) inner and outer relative bearing eccentricities; (c) rotor and ring speed.

a stable equilibrium position. At $t \approx 1800$ ms, the rotor becomes unstable and reaches a stable limit cycle. The simulation shows that the bifurcation is induced by the inner oil films (large increase of the inner relative bearing eccentricity ε_i). Hence, the subsynchronous frequency is generated by the inner *oil whirl/whip*. Note that because of the damping effect of the outer fluid films, the inner bearing eccentricities ε_i remain well below 1. Moreover, due to the damping of the outer fluid films, the inner *oil whirl/whip* can be passed through and the system becomes stable again at $t \approx 4500$ ms. The rotor remains stable up to $t \approx 7300$ ms, where the outer fluid films get unstable (the simulation shows a large increase of the outer relative bearing eccentricity ε_o). The outer *oil whirl/whip* gives rise to a stable limit cycle oscillation; the amplitudes remain moderate, since the outer *oil whirl* is damped due to the inner fluid films.

A.3. Run-up simulation of a turbocharger in full-floating ring bearings

Finally, we present a run-up simulation carried out with a flexible multibody model of the examined turbocharger of Section 2. The rotor speed is steadily increased up to 2700 Hz. A frequency spectrum of the *y*-displacement of the measurement point (see Fig. 2) is depicted in Fig. 20, which also shows the inner and outer relative bearing eccentricities of the compressor-sided (ε_{C_i}, ε_{C_o}) and turbine-sided (ε_{T_i}, ε_{T_o}) ring. As can clearly be seen, the *1. Subsynchronous* is induced by the inner fluid films (significant increase in ε_{C_i} and ε_{T_i}). The simulations further show that the inner *oil whirl* excites the *gyroscopic conical forward mode*. The *2. Subsynchronous* is also related to the *oil whirl* of the inner fluid films, which now excite the *gyroscopic translational forward mode*. The simulated bifurcation sequence correlates with Measurement 5. Please note that in the computer model no mixed friction approach has been implemented. Therefore, the simulation does not show the start of ring rotation according to Fig. 13.

Further simulations with different system and operating parameters also exhibit the *3. Subsynchronous*. These simulations clearly show that the *3. Subsynchronous* is induced by the outer *oil whirl/whip*, which excites the *gyroscopic conical forward mode*.

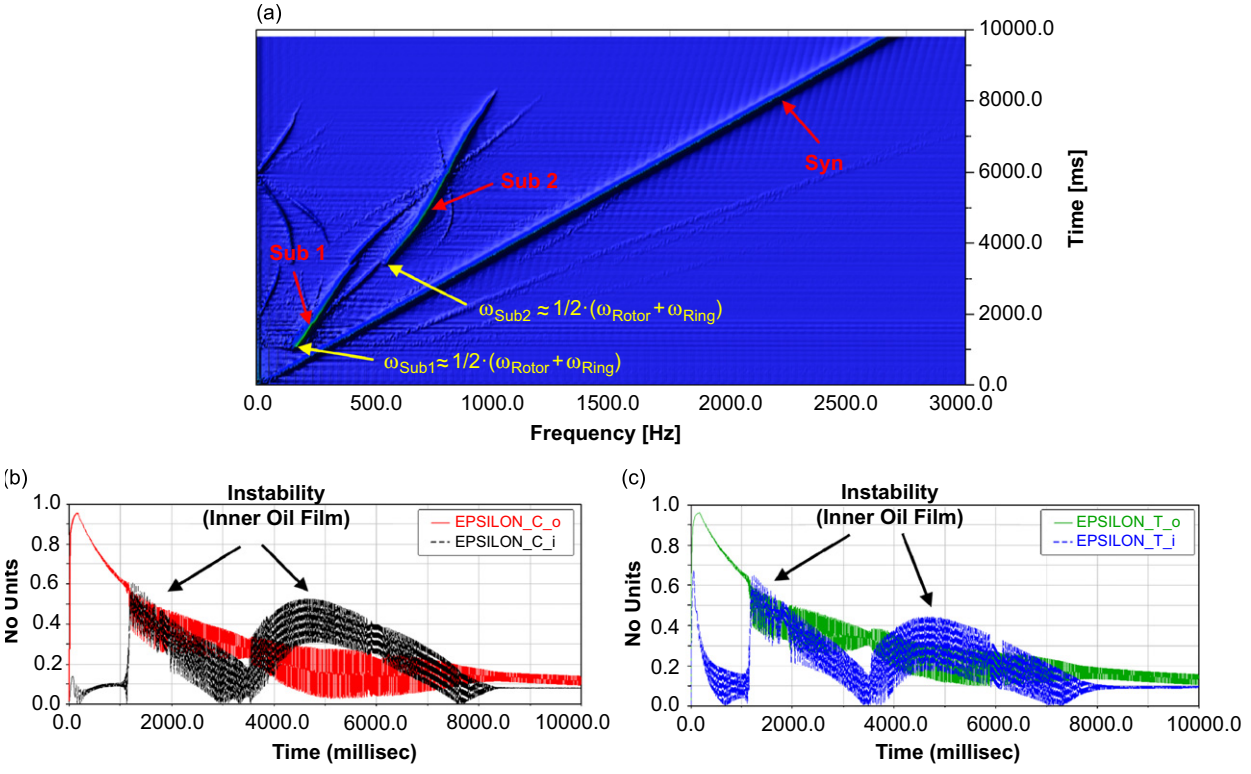

Fig. 20. Run-up simulation of the turbocharger; (a) frequency spectrum of *y*-displacement of measurement point; (b), (c) inner and outer relative bearing eccentricities of the compressor-sided and turbine-sided ring.

References

[1] R. Gasch, R. Nordmann, H. Pfützner, *Rotordynamik (Rotor Dynamics)*, Springer, Berlin, 2002.
[2] P.C. Müller, Allgemeine lineare Theorie für Rotorsysteme ohne oder mit kleinen Unsymmetrien (General linear theory without or with small asymmetries), *Ingenieur-Archiv (Archive of Applied Mechanics)* 51 (1981) 61–74.
[3] J.S. Rao, *Rotor Dynamics*, Wiley, New York, 1991.
[4] H.R. Born, Analytical and experimental investigation of the stability of the rotor-bearing system of a new small turbocharger, *Gas Turbine Conference*, ASME Paper 87-GT-110, Anaheim, CA, USA, 1987.
[5] B. Domes, Amplituden der unwucht- und selbsterregten Schwingungen hochtouriger Rotoren mit rotierenden und nichtrotierenden schwimmenden Buchsen (Amplitudes due to Imbalance and Self-excited Oscillations of High-Speed Rotors in Full- and Semi-Floating Ring Bearings), PhD Thesis, University of Karlsruhe, Germany, 1980.
[6] C. Holt, L. San Andres, Test response and nonlinear analysis of a turbocharger supported on floating ring bearings, *Journal of Vibration and Acoustics* 127 (2005) 107–115.
[7] M. Loos, R. Wohlrab, Experimentelle und theoretische Untersuchungen zum Einfluß der Gestaltung der Gleitlagerung auf das Stabilitätsverhalten eines Turboladerrotors (Experimental and theoretical investigations on the influence of the bearing design on the stability of turbochargers), VDI Report, Vol. 20, 1992, pp. 139–152.
[8] A. Meyer, Äußere Lagerdämpfung für sehr hochtourige, gleitgelagerte Rotoren (Outer Bearing Damping for High-Speed Rotors in Hydrodynamic Bearings), PhD Thesis, University of Karlsruhe, Germany, 1987.
[9] L. San Andres, J.C. Rivadeneira, K. Gjika, C. Groves, G. LaRue, A virtual tool for prediction of turbocharger nonlinear dynamic response: validation against test data, *Proceedings of ASME Turbo Expo 2006, Power for Land, Sea and Air*, 08–11 May, Barcelona, Spain, 2006.
[10] L. San Andres, J. Kerth, Thermal effects on the performance of floating ring bearings for turbochargers, *Proceedings of the Institution of Mechanical Engineers Part J: Journal of Engineering Tribology* 218 (2004) 437–450.
[11] J. Trippet, D. Li, High-speed floating-ring bearing test and analysis, *ASLE Transactions* 27 (1983) 73–81.
[12] A. Muszynska, Whirl and whip—rotor/bearing stability problems, *Journal of Sound and Vibration* 110 (3) (1986) 443–462.
[13] A. Muszynska, Tracking the mystery of oil whirl, *Sound and Vibration* February (1987) 8–12.
[14] A. Muszynska, Stability of whirl and whip in rotor/bearing systems, *Journal of Sound and Vibration* 127 (1) (1988) 49–64.
[15] A. Muszynska, The fluid force model in rotating machine clearances identified by modal testing and model applications: an adequate interpretation of the fluid-induced instabilities, *Iscorma-2, International Symposium on Stability Control of Rotating Machinery 2001*, South Lake Tahoe, CA, USA.
[16] T. Someya, Stabilität einer in zylindrischen Gleitlagern laufenden unwuchtfreien Welle (Stability of a rotor without imbalance in plain hydrodynamic bearings), *Ingenieur-Archiv (Archive of Applied Mechanics)* 23 (1963) 85–108.
[17] T. Someya, Schwingungs- und Stabilitätsverhalten einer in zylindrischen Gleitlagern laufenden Welle mit Unwucht (Vibrations and stability behavior of a rotor with imbalance in plain hydrodynamic bearings), *VDI-Forschungsheft* 510 (1965) 5–36.
[18] J.W. Lund, Stability and damped critical speeds of a flexible rotor in fluid film bearings, *Journal of Engineering for Industry—ASME* 10 (1974) 509.
[19] P. Hagedorn, *Nonlinear Oscillations*, second ed., Oxford University Press, Clarendon Press, 1988.
[20] K. Magnus, K. Popp, Schwingungen (Oscillations), Teubner Verlag, 7, Auflage, 2005.
[21] A.H. Nayfeh, D.T. Mook, Nonlinear Oscillations, Wiley-Interscience, Reprint Edition, 1995.
[22] A. Shabana, *Dynamics of Multibody Systems*, Cambridge University Press, Cambridge, 2005.
[23] Z. Guo, R.G. Kirk, Instability boundary for rotor-hydrodynamic bearing systems—part 1: Jeffcott rotor with external damping, *Journal of Vibration and Acoustics* 125 (4) (2003) 417–422.
[24] Z. Guo, P.G. Kirk, Instability boundary for rotor-hydrodynamic bearing systems—part 2: rotor with external flexible damped support, *Journal of Vibration and Acoustics* 125 (4) (2003) 423–426.
[25] C.J. Myers, Bifurcation theory applied to oil whirl in plain cylindrical journal bearings, *ASME Journal of Applied Mechanics* 51 (1984) 244–250.
[26] A. Cameron, *Basic Lubrication Theory*, Horwood, 1981.